Appl. Phys. A 68, 597–602 (1999) / DOI 10.1007/s003399900024

Applied Physics A
Materials
Science & Processing

Thermoelectric properties of mechanically alloyed Bi–Sb alloys

R. Martin-Lopez[1], A. Dauscher[1], H. Scherrer[1], J. Hejtmanek[2], H. Kenzari[1], B. Lenoir[1]

[1] Laboratoire de Physique des Matériaux, UMR 7556 CNRS-UHP-INPL, Ecole des Mines, Parc de Saurupt, 54042 Nancy, France
(Fax: +33-3/8357-9794, E-mail: dauscher@mines.u-nancy.fr)
[2] Institut of Physics, Division of Solid State Physics, Cukrovarnická 10, 16200 Prague, Czech Republic

Received: 11 November 1998/Accepted: 5 January 1999/Published online: 24 March 1999

Abstract. Homogeneous polycrystalline $Bi_{100-x}Sb_x$ ($x = 12$, 15, 22) alloys were synthesized by mechanical alloying. The transport coefficients (electrical resistivity, thermal conductivity, and thermopower) were measured, in the 77–300 K temperature range, on samples consolidated either by sintering or extrusion. The thermoelectric figure of merit was deduced from the three coefficients. The temperature dependences are discussed as a function of the alloys' microstructures taking into account the qualitative effect of potential barriers. Extrusion leads to better performing thermoelectric materials than does sintering. The highest figure of merit is reached for temperatures around 150 K, a temperature at which no reliable thermoelectric material of long service life is available until now.

PACS: 72.15.Jf; 81.20.Ev

Cryogenic solid-state Peltier coolers are connected with advanced thermoelectric systems operating at temperature down to ≈ 100 K for military and civilian applications. In particular, cryoelectronics and "cold computing" are emerging fields requiring reliable, low maintenance of cooling technology with long-term service life.

Desirable qualities for thermoelectric materials include a large thermoelectric power α, a small electrical resistivity ρ, and a small thermal conductivity λ. These transport coefficients determine the so-called thermoelectric figure of merit Z [1], which has the dimensions of an inverse temperature (K^{-1}):

$$Z = \frac{\alpha^2}{\rho\lambda} \,. \tag{1}$$

Bismuth is a (group V) semimetal that crystallizes in the spatial group $R\bar{3}m$ and exhibits a layered structure. It possesses a small energy overlap between the conduction and valence bands, high carrier mobilities, and small effective masses. By alloying bismuth with small amounts of antimony, the energy overlap decreases. According to the band structure determined at $T \cong 0$ K, Bi–Sb alloys containing between 7 and 22 at. % Sb are semiconductors [2–4], and are classified as narrow band-gap semiconductors since their thermal gap does not exceed 25 meV. Above 22 at. % Sb and below 7 at. % Sb, Bi–Sb alloys are semimetals.

Up to now properly oriented semiconducting single crystals of $Bi_{100-x}Sb_x$ have been found to be the best n-type thermoelectric materials for low-temperature (80 K) thermoelectric cooling when current flows along the trigonal axis [5, 6]. However, the propensity of Bi–Sb single crystals to cleave along the basal planes drastically limits their use in thermoelectric devices.

Although there is no doubt that $Bi_{100-x}Sb_x$ single crystals have thermoelectric figures of merit superior to those displayed by polycrystalline materials, there are practical advantages in using samples produced by powder metallurgy. Such advantages include speed of preparation, consistency of composition, and mechanical strength.

Among powder metallurgy processings, mechanical alloying (MA) of the raw materials is a very effective method to obtain fine-grained solid solutions of thermoelectric materials. It has been succesfully applied to fabricate Si–Ge alloys [7], $(Bi, Sb)_2(Te, Se)_3$ based materials [8, 9] and Bi–Sb alloys [10]. MA is a particularly suitable, simple and cost-saving mass-production method allowing one to quickly achieve homogeneous Bi–Sb alloys, compared with the conventional "vacuum melting/grinding" process. During MA, the alloys are formed from the elemental materials through a sequence of collision events in a high-energy ball mill [11].

Obtaining fine grains ($< 10\,\mu$m) is very important in particular from the point of view of the processing of advanced thermoelectric materials. Grain refinement reduces the lattice thermal conductivity due to phonon scattering by grain boundaries [12, 13], and as a consequence improves the figure of merit. The manner of forming (hot pressing, cold pressing and annealing, extrusion, etc...) and its processing conditions may also strongly affect the microstructure. For instance, forming the material by extrusion may introduce a preferential orientation of the grains in the consolidated material. The presence of a strong texture in a layered material such as Bi–Sb alloys would be favorable from a thermoelectric point of view. Actually, if all the grains could be oriented so

that their trigonal axes are nearly parallel, then their thermoelectric properties should approach those of single crystals. Banaga et al. [14], by studying the hot extrusion of a $Bi_{88}Sb_{12}$ polycrystalline alloy with a rod of small diameter (1–5 mm), observed a strong texture with the trigonal axis of the alloy along the extrusion direction. They reported figures of merit slightly higher than those for the average values of the figure of merit of a single crystal of the same composition.

The present work reports on the thermoelectric properties of homogeneous alloys of $Bi_{100-x}Sb_x$ ($x = 12$, 15, 22) prepared by MA. The electrical resistivity, the thermoelectric power, and the thermal conductivity were measured on either sintered ($x = 12$, 15, 22) or hot extruded ($x = 15$) samples within the temperature range 77–300 K. The figure of merit was calculated from the measured values using (1). Influence of both the antimony content and the consolidation method on the modification of the thermoelectric properties with temperature is discussed.

1 Experimental procedure

Mechanical alloying was conducted in a planetary ball mill (Fritsch, Pulverisette 5) with balls (diameter = 30 mm) and jars (250 ml) of hardened stainless steel. The rotation speed of the plateau was fixed at 236 rpm. A ball-to-powder weight ratio (BPR) of 10:1 was used.

Base bismuth and antimony of high purity (99.999%) with initial particle sizes of 10 mm were introduced in the vessels in a stoichiometric ratio ($Bi_{100-x}Sb_x$, $x = 12, 15, 22$) under an argon atmosphere in a glove box. The vessels were then hermetically sealed in order to prevent a possible oxidation of the materials during ball milling.

X-ray diffraction (XRD) analyses of the powder samples were performed in a Siemens D-500 diffractometer with Co-$K_{\alpha 1}$ radiation, in the standard $\theta - 2\theta$ geometry in order to follow the structural modification of the powders during the MA. The micro-homogeneity of the ball-milled powders was determined by microprobe analyses (CAMEBAX SX 50). For this purpose, the powder samples were compacted first under a uniaxial pressure of 500 MPa during 2 min and then polished at 1 μm with alumina powders. Chemical analysis determined the amount of impurities introduced in the powders during the ball milling.

The material was formed following two different methods: sintering and extrusion. For sintering, the ball-milled powders were first compacted in the form of cylindrical greens of 10 mm in diameter under a uniaxial pressure of 160 MPa, then submitted to a thermal treatment in a furnace at 250 °C during 60 min under a He–H_2 atmosphere. The $Bi_{85}Sb_{15}$ alloy was extruded at 265 °C with a 2.5 extrusion ratio from cylindrical greens of 25 mm in diameter, which yielded estimated density of 75% of the theoretical density.

The microstructure of the sintered and extruded samples was studied by scanning electron microscopy (SEM) in a JEOL JMS 820 in the secondary-electron image mode. The samples were etched by electrochemical polishing.

Prior to the measurement of the transport properties, the sintered and extruded samples were cut with a wire saw into parallelepipeds (typical dimensions were $2.5 \times 2.5 \times 10$ mm).

Because of the strong anisotropy of the Bi−Sb single crystals, we calculated average values of the transport coefficients, measured both along the trigonal axis and the basal planes, of a single crystal of $Bi_{85}Sb_{15}$ [6]. We compared this set of data with data for our polycrystalline $Bi_{85}Sb_{15}$ samples.

Electrical resistivity, thermoelectric power, and thermal conductivity were measured on the same samples, between 77 K and 300 K. Both the thermal (thermoelectric power and thermal conductivity) and electric (electrical resistivity) gradients were applied along the extrusion direction for the extruded material, and perpendicular to the press direction for the sintered materials. Thermal transport was measured using a steady-state method. A schematic view of the experimental setup is shown in Fig. 1. One end of the bar-shaped sample was soldered by means of Bi−Sn compound to a piece of copper thermally anchored to the heat sink of the cryostat, but electrically insulated from it. The other end of the sample was provided with a small heater to generate the heating current. The resulting gradient (typically 1.5 K) along the sample length was measured using two differential chromel–constantan thermocouples (0.072 mm in diameter) that were soldered to two small copper tabs, which were soldered to the sample with Bi−Sn compound. The potential difference arising from the thermoelectric power was measured using the chromel wires. The electrical resitivity was measured prior to energizing the heater by means of a direct-current four-probe method. Care was taken to eliminate any thermoelectric voltages by reversing the direction of the current for each measurement. Current leads were soldered to two copper tabs attached near the ends of the sample. This experimental setup in respect of thermal conductance of used specimens ensured that the heat resistance of current leads and thermocouples exceeds by two orders of magnitude the thermal resistance of the specimen. The main problem is the radiative losses. These can be, however, calculated and extracted from the measured values.

Let us underline that a choice of materials used for current, thermal, and potential leads represents a compromise between the contradictory requirements for a low thermal conductance versus a low thermoelectric power of thermocouples or leads. The use of chromel–constantan thermocouples and chromel wires as a potential and current leads have

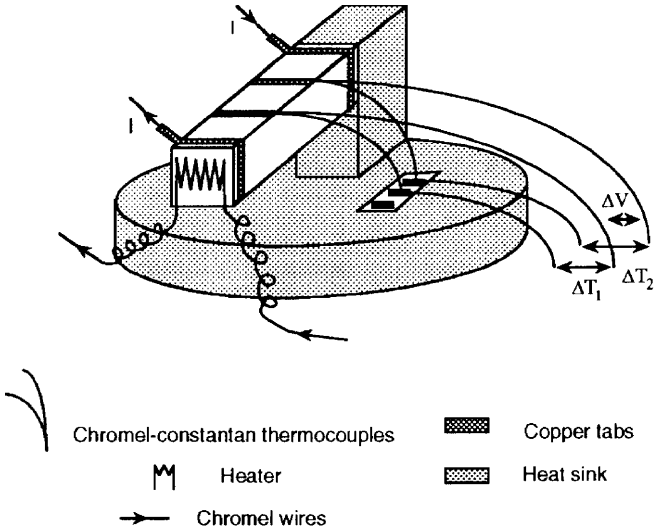

Fig. 1. Schematic representation of the sample holder used to measure the electrical resistivity, the thermoelectric power, and the thermal conductivity from 77 to 300 K

been justified on the thermal and transport measurements on single-crystalline $Bi_{100-x}Sb_x$ alloys [15]. Prior to the measurements on the sintered and extruded samples we checked the reliability of our measuring technique using the previously measured specimens, and the measured temperature dependencies of all physical characteristics perfectly (±2%) coincide within the 80–300 K temperature range. Naturally, careful corrections to the radiation losses and thermoelectric power of chromel (Omega tables) have been made. In the case of electrical resistivity the high speed of measuring cycle, i.e. ≈ 1000 ms for both the current reverse and potential offsets measurements before and after the measurement, with respect to the thermal relaxation constant $\tau_p \approx 100$ s enabled us to eliminate the parasitic effects.

We also extended the electrical resistivity measurement of the sintered ($x = 12$, 15) and extruded samples ($x = 15$) from 6 to 280 K in another experimental setup. In this system, the sample was in good thermal contact with the heat sink. Here also, the voltage was rapidly measured after the application of the electrical current. For two samples measured in both experimental setups, the measured temperature dependencies of the electrical resistivity perfectly coincide within the 80–280 K temperature range.

2 Results and discussion

2.1 Sample characterization

XRD analyses showed that the sought $Bi_{100-x}Sb_x$ alloys were reached after about 15 h of milling time for $x = 12$ and 15 whereas 25 h was necessary for $x = 22$. A more detailed description of the alloy formation during the milling process has been presented elsewhere [16]. Although the diffraction patterns show no contamination from the vessels or balls, impurities were found from chemical analysis. The results reveal the presence of Fe, Ni, and Cr. The values, in ppm, are located in the following intervals: [55–60], [12–15], and [29–33] for Fe, Ni, and Cr, respectively. These values differ slightly according to the sample preparation and content. There is however no clear dependence of the contamination step on the milling time or on the antimony content.

The microprobe analyses show that the mechanically milled powders are very homogeneous in antimony content. As an example, Fig. 2 shows the electron microprobe analysis of a $Bi_{85}Sb_{15}$ sample: less than 1 at. % variation in the mean antimony concentration was achieved.

The sintered samples exhibited a microstructure with randomly oriented grains as confirmed by texture analyses. The grains had sizes ranging from 2 to 10 μm. In some grains, parallel broad lines corresponding to the cleavage planes of each single grain could be observed (Fig. 3).

The original shape of the extruded material was a cylindrical bar which showed a smooth external surface without any damage. This bar was cut to observe the microstructure in both parallel and perpendicular directions to the extrusion direction. The grains had sizes ranging from 2 to 30 μm and they seemed randomly oriented, as can be observed in Fig. 4. However, texture analyses revealed two preferential orientations in the sample: the [012] and the [110] directions (in reduced hexagonal notation), both being parallel to the extrusion direction. We must point out that Banaga et al. [14]

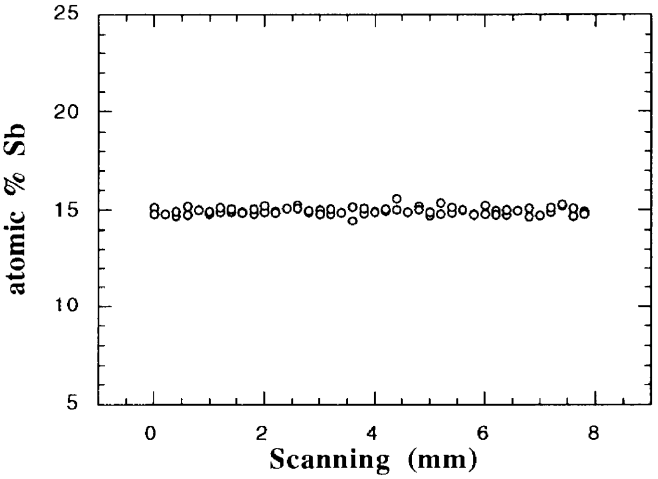

Fig. 2. Microprobe scanning along a line of 8 mm in length of a $Bi_{85}Sb_{15}$ compacted sample (BPR 10:1 and milling time 15 h), showing the obtaining of the expected composition with an homogeneity better than 1 at. %

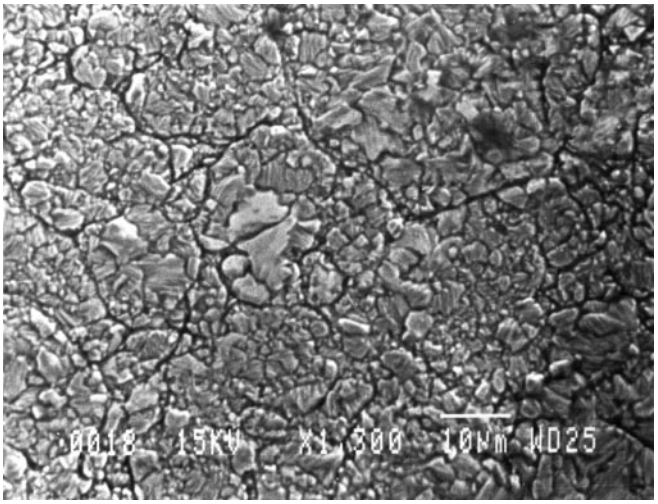

Fig. 3. Microstructure of the sintered samples ($x = 15$). The micrograph is taken from a sample cut parallel to the pressing direction. Note the presence of lines corresponding to the cleavage planes

obtained an extruded $Bi_{88}Sb_{12}$ material with a strong texture in the [001] direction (trigonal axis), parallel to the extrusion direction. Instead of this result, the structural peculiarities of our extruded samples are consistent with the theory and practice of deformation of layered materials, which predict that the trigonal axis should be perpendicular to the extrusion direction.

2.2 Transport properties

The temperature dependences of the electrical resistivity of both extruded and sintered samples within the 77–300 K temperature range are shown in Fig. 5. The computed average values obtained with a $Bi_{85}Sb_{15}$ single crystal are also reported in this figure. (Note that in this case the anisotropy (ρ_{11}/ρ_{33}) is less than 1.3 between values measured along (ρ_{33}) or perpendicular (ρ_{11}) to the trigonal axis).

The electrical resistivity of all polycrystalline samples increases with decreasing temperature and displays an activated

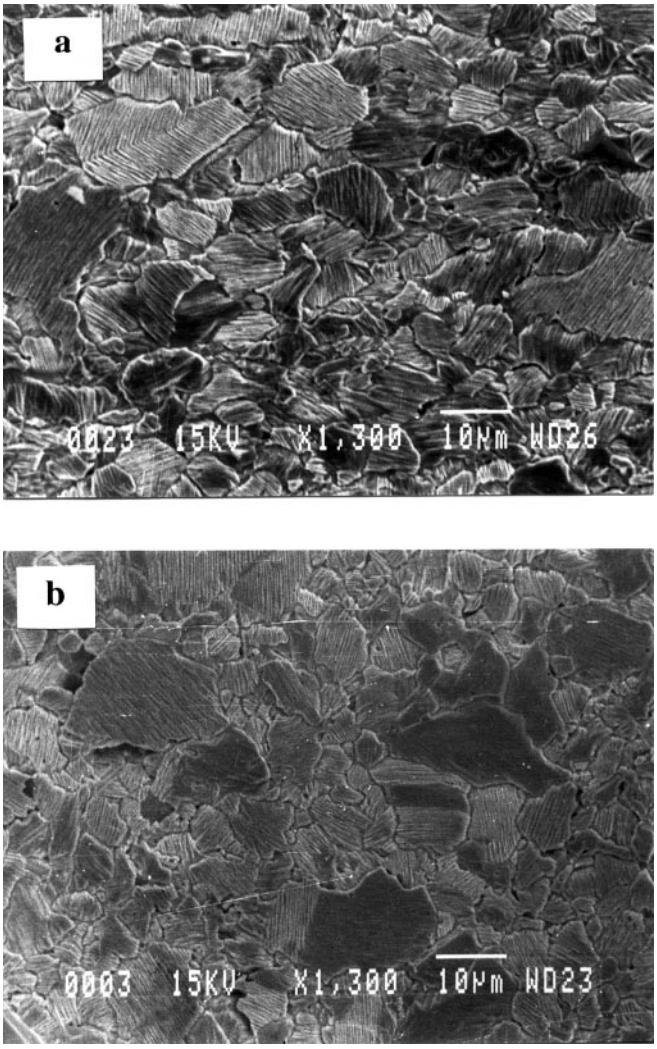

Fig. 4a,b. Microstructure of the extruded samples ($x = 15$). **a** Along the extrusion direction. **b** Perpendicular to the extrusion direction. Note again the presence of lines corresponding to the cleavage planes

behaviour. It differs from $\rho(T)$ of the single crystal of same composition because of higher values of the resistivity and the fact that the activated behavior begins at room temperature or even higher. Estimation of the activation energy E_g can be calculated assuming the relation:

$$\rho \propto \exp\left(\frac{E_g}{2KT}\right) , \qquad (2)$$

where K is the Boltzman constant and T the absolute temperature.

The estimated activation energies, lying between 20–35 meV, are higher than those reported for the single crystal [17]. We believe that the higher values of both the electrical resistivity and the activation energy can be qualitatively explained by the presence of potential barriers in the intergranular regions. Due to the method of material preparation, the boundary regions may contain a large number of impurities or point or line defects. If carriers become localized at these boundaries, these charged boundaries could then act as potential barriers that would prevent the flow of free carriers.

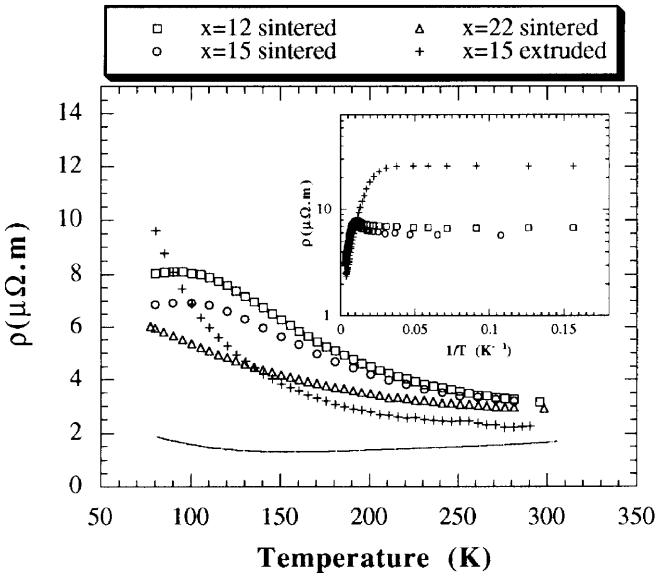

Fig. 5. Temperature dependence of the electrical resistivity of sintered and extruded samples between 77–300 K. (—) represents the computed average values for a single crystal ($x = 15$). The behavior below 77 K is shown in the inset for $x = 12$ and 15

Measurements extended below 77 K are reported in the inset of Fig. 5, for $x = 12$ and $x = 15$. The temperature-independent behavior below 77 K indicate a metallic behavior, observed whatever the sample. This result is not surprising when taking into account the high impurity level in our samples. Actually, in Bi−Sb alloys, the effective Bohr radii of impurities are very large ($\approx 10^{-4}$ cm) on account of the small electronic effective masses. Thus the impurities' wave functions tend to overlap each other, so that the impurities band can be considered as merged in the conduction or the valence band even in the purest materials available (for Bi−Sb the critical concentration of impurities for which there are bound states is less than 10^{12} cm^{-3}). Nevertheless, it should be noted that the electrical resistivities at temperatures below 80 K are higher in the extruded material than in the sintered alloy and the average values in a single crystal. The potential barriers introduced in the material by extrusion seem to act more efficiently on the charge carriers than do the potential barriers of the sintered materials, and as a consequence the electrical resistivities in this temperature range increase.

In Fig. 6, thermoelectric power values are plotted as a function of temperature for sintered and extruded samples. They are negative for all samples in the temperature range investigated. This fact reflects the higher mobilities of electrons compared to those of holes.

For sintered samples, the absolute values of the thermoelectric power increase with decreasing temperature up to a maximum value for a temperature near 150 K. The smaller values of the absolute thermoelectric power for $x = 22$ with respect to $x = 12$ or $x = 15$ reflect the more pronounced semimetallic behavior of this alloy. In the extruded sample, the maximum of the absolute value of thermoelectric power is shifted towards lower temperature ($T = 100$ K), causing the absolute thermoelectric power values to be increased by comparison with those obtained on the sintered sample for $T < 140$ K.

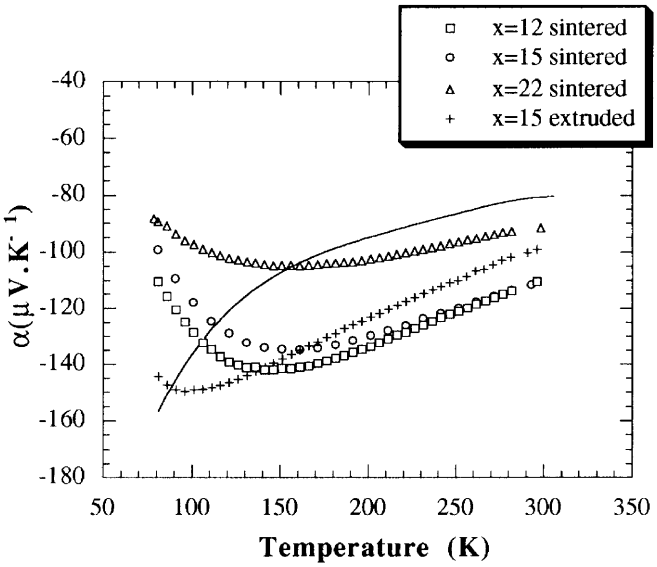

Fig. 6. Temperature dependence of the thermopower of sintered and extruded samples between 77–300 K. (—) represents the computed average values for a single crystal ($x = 15$)

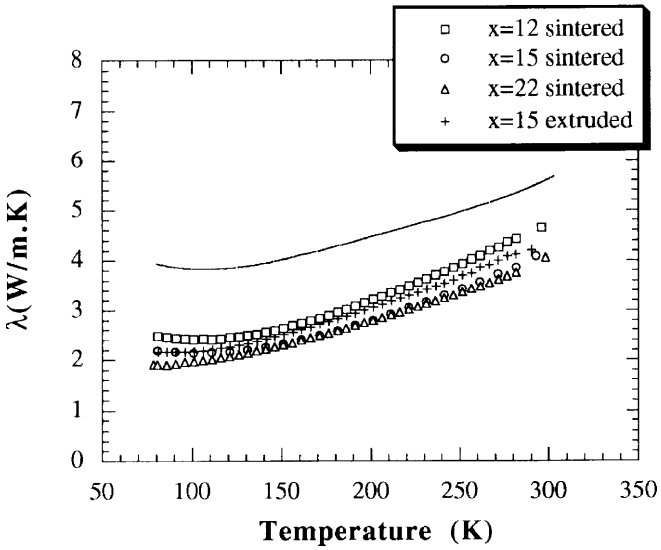

Fig. 7. Temperature dependence of the thermal conductivity of sintered and extruded samples between 77–300 K. (—) represents the computed average values for a single crystal ($x = 15$)

It should be noted that the absolute values of the thermoelectric power of the extruded polycrystalline samples lie entirely above the average values of a single crystal of the same composition (the thermoelectric power is roughly isotropic for $7 < x < 22$ in the 80–300 K temperature range for single crystals) [6]. Such a behavior was already mentioned by Banaga et al. for hot extruded $Bi_{88}Sb_{12}$ alloys [14]. The increased absolute value of the thermopower could be linked to a decreased relaxation time of charge carriers due to additional scattering mechanisms leading to an increase of the scattering parameter. Scattering by potential barriers could contribute significantly. Actually, for barrier heights close to the Fermi energy, the barriers should scatter strongly the carriers whose energies are lower than the Fermi value and much less strongly scatter those with energies above the Fermi level. This could reduce the energy of the charge carrier flux and increase the thermoelectric power [18, 19].

In Fig. 7 are represented the temperature dependences of the thermal conductivity of both extruded and sintered samples. The behavior is similar for each sample, the thermal conductivity values decrease when temperature diminishes and stabilize below around 100 K. The computed average values of the thermal conductivity of a single crystal of $Bi_{85}Sb_{15}$ are also reported (the anisotropy is near 1.7 in Bi−Sb single crystals). The temperature dependence of the single crystal follows the same trends as those of the polycrystalline samples but the thermal conductivities are about twice greater.

In Bi−Sb alloys, the thermal conductivity λ is principally the sum of two terms: an electronic contribution λ_E (including both unipolar and bipolar terms) and a contribution λ_L associated with the lattice phonons:

$$\lambda = \lambda_E + \lambda_L \, . \tag{3}$$

In our polycrystalline alloys the thermal conductivity is principally due to the lattice contribution below the Debye temperature θ_D ($\theta_D = 120$ K in Bi) [20]. At higher temperature ($T > \theta_D$) the electron and phonon components are comparable in magnitude. In single crystals, the electronic component can be estimated by use of the Wiedeman–Franz law:

$$\lambda_E = LT/\rho \, , \tag{4}$$

with $L = 2.44 \times 10^{-8}\,V^2K^{-2}$.

As might be expected, below θ_D the heat is primarily transported by phonons, but at higher temperatures the electronic component becomes more important. The reduction of the lattice conductivity in the consolidated powder below θ_D results from additional scattering of phonons by defects that have been introduced during the powder-metallurgy process.

Theoretically, a substantial reduction of λ_L is also expected at higher temperatures in the polycrystalline solid solution due to the scattering of the low-frequency phonons at grain boundaries when the grain sizes are less than 5 μm [13]. The physical reason is that high-frequency phonons are strongly scattered by point defects in the solid solution, leaving most of the heat to be carried by the low-frequency phonons, which have very long mean-free-paths. These phonons are thus much more likely able to scatter at grain boundaries. Experimentally, it has been shown that the decrease occurs for grain sizes somewhat larger than those expected by the theory [21].

From the measurements of the three transport coefficients α, ρ, and λ, we deduced the values of the figure of merit Z. The temperature dependences of the figure of merit of both extruded and sintered samples, reported in Fig. 8, exhibit quasi-similar behaviors. The figure of merit increases slowly from 300 K up to a maximum for temperatures around 140–180 K and then drops for lower temperatures. Compared to single crystals, the maximum is shifted from 70 K towards higher temperatures. The highest figure of merit of the sintered alloys corresponds to $x = 15$, with a value of $1.4 \times 10^{-3}\,K^{-1}$ at 170 K. It is clearly seen that the consolidation by extrusion has a favourable effect on Z compared to the effect of sintering in the temperature range investigated. Moreover, taking into account the fact that the mechanical

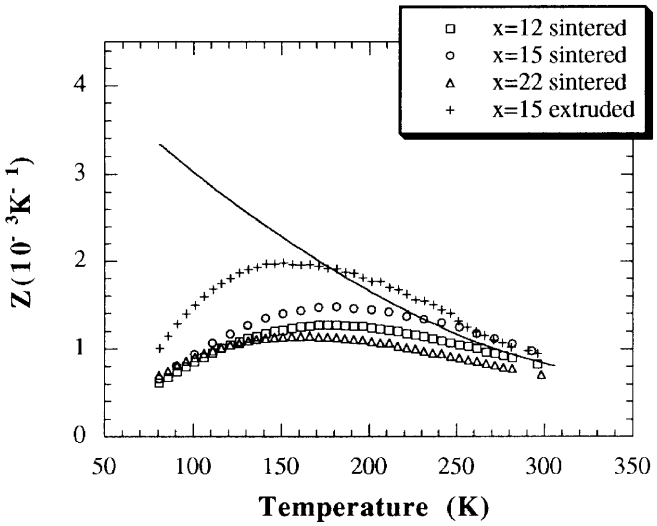

Fig. 8. Temperature dependence of the figure of merit of sintered and extruded samples between 77–300 K. (—) represents the computed average values for a single crystal ($x = 15$)

strength of the polycrystalline Bi−Sb alloys is about one order of magnitude higher than that of single crystals [22], and, that their thermoelectric performances are equal or even higher for temperatures greater than 160 K, the use of polycrystalline Bi−Sb alloys becomes of great interest in a temperature range not exploited until now because of lack of suitable material.

3 Conclusion

The temperature dependences of the electrical resistivity, the thermoelectric power, the thermal conductivity, and thus the thermoelectric figure of merit were investigated between 77 and 300 K (4–300 K for the electrical resistivity) on homogeneous polycrystalline $Bi_{100-x}Sb_x$ alloys prepared by mechanical alloying. For $x = 12$ and 15, semiconducting behaviors were observed, whereas for $x = 22$, results indicate a more like semimetallic behavior, in agreement with the band structure of these alloys.

The higher electrical resistivities and absolute thermoelectric powers obtained with the polycrystalline samples in comparison with those of single crystals have been explained by the presence of potential barriers introduced by the powder-metallurgy process.

Scattering of low-frequency phonons at the grain boundaries lowers the thermal conductivity. This lowering is however not enough to compensate the enhancement of the electrical resistivity, leading to a decrease of the figure of merit. Because of the shift of the figure of merit towards higher temperature in the polycrystalline samples, especially when they are formed by extrusion, these Bi−Sb alloys become interesting materials between 150 K and room temperature, particularly since their mechanical strength is nearly 6 times better in this temperature range.

The extrusion process could moreover be optimised in order to introduce a unique texture in the material.

Acknowledgements. The authors would like to thank J.-P. Haeussler for his assistance in microprobe analyses, M. Zandona for the X-Ray diffraction analyses, and Prof. B. George and Dr. C. Bellouard for measurements of low-temperature electrical resistivity. The authors are also very indebted to Dr. O.N. Uryupin, Dr. V.M. Grabov, and Prof. A. Casian for fruitful discussions.

References

1. A.F. Ioffe: *Semiconductor Thermoelements and Thermoelectric Cooling* (Infosearch, London 1957) p. 39
2. E.J. Tichovolsky, J.G. Mavroides: Solid State Commun. **7**, 927 (1969)
3. P.W. Chao, H.T. Chu, Y.H. Kao: Phys. Rev. B **9**, 4030 (1974)
4. G. Oelgart, G. Schneider, W. Kraak, R. Herrmann: Phys. Status Solidi B **74**, K75 (1976)
5. G.E. Smith, R. Wolfe: J. Appl. Phys. **33**, 841 (1962)
6. W.M. Yim, A. Amith: Solid State Electronics **15**, 1141 (1972)
7. R.M. Davis, C.C. Koch: Scripta Metall. **21**, 305 (1987)
8. P. Pierrat, A. Dauscher, B. Lenoir, R. Martin-Lopez, H. Scherrer: J. Mater. Sci. **32**, 3653 (1997)
9. K. Hasezaki, M. Nishida, M. Umata, H. Tsukuda, M. Araoka: Mater. Trans. JIM **35**, 428 (1994)
10. R. Martin-Lopez, M. Zandona, H. Scherrer: J. Mater. Sci. Lett. **15**, 16 (1996)
11. C. Koch, R.W. Cahn, P. Haasen, E.J. Kramer: Mater. Sci. Technol. **7**, 97 (1991)
12. H.J. Goldsmid, A.W. Penn: Phys. Lett. **27**, 523 (1968)
13. H.J. Goldsmid, H.B. Lyon Jr. and E.H. Volckmann: Proceedings of the XIV International Conference on Thermoelectrics (St Petersburg, Russia 1995) p. 71
14. M.P. Banaga, O.B. Sokolov, T.E. Benderskaya, L.D. Dudkin, A.B. Ivanova, I.I. Fridman: Neorg. Mater. **22**, 619 (1986)
15. M. Cassart, E. Grivei, J.-P. Issi, E. Ben Salem, B. Chevalier, C. Brisson, A. Tressaud: Physica C **213**, 327 (1993)
16. R. Martin-Lopez, B. Lenoir, A. Dauscher, X. Devaux, W. Dümmler, H. Scherrer, M. Zandona, J.F. Remy: Scripta Mat. **37**, 219 (1997)
17. B. Lenoir, A. Dauscher, X. Devaux, R. Martin-Lopez, Yu.I. Ravich, H. Scherrer, S. Scherrer: Proceedings of the XV International Conference on Thermoelectrics (Pasadena, USA 1996) p. 1
18. Yu.I. Ravich: *CRC Handbook of Thermoelectrics* (CRC Press, Florida 1995) p. 67
19. Y. Nishio, T. Hirano: Jpn. J. Appl. Phys. **36**, 170 (1997)
20. V.D. Kagan, N.A. Red'ko: Sov. Phys. JETP **73**, 664 (1991)
21. E.H. Volckmann, H.J. Goldsmid, J. Sharp: Proceedings of the XV International Conference on Thermoelectrics (Pasadena, USA 1996) p. 22
22. R. Martin-Lopez, S. Zayakin, B. Lenoir, F. Brochin, A. Dauscher, H. Scherrer: Philos. Mag. Lett. **78**, 287 (1998)